Earthquake Geotechnical Engineering for Protection and Development of Environment and Constructions – Silvestri & Moraci (Eds)
© 2019 Associazione Geotecnica Italiana, Rome, Italy, ISBN 978-0-367-14328-2

Evaluation of constitutive law applicability for the ground improvement by jet grouting

J. Kawamura & Y. Iguchi
Chemical Grouting Co. Ltd., Tokyo, Japan

T. Namikawa
Shibaura Institute of Technology, Tokyo, Japan

K. Takehara
JIP Techno Science Corporation, Tokyo, Japan

T. Yamada & S. Ohno
Kajima Corporation, Tokyo, Japan

ABSTRACT: Ground improvement based on the introduction of a lattice structure by jet grouting is widely adopted to prevent seismic liquefaction phenomena. Conventional design prescribes that the allowable stress of an improved body should remain within the range of elastic behavior during an earthquake, but the characteristics of phenomena associated with improved ground after earthquake-related failure remain unclear. Against this background, Namikawa and Mihira (2007) proposed an elasto-plastic constitutive law capable of expressing strain-softening/hardening response after tensile and shear failure. In the present study, the authors simulated an unconfined compression test with a previously described elasto-plastic model for large-scale core sampling of a body improved via jet grouting to verify the model's applicability. FEM analysis was subsequently conducted to evaluate the resistance of improvement based on a lattice structure with local failure against a strong earthquake.

1 INTRODUCTION

In conventional design for improvement based on a lattice structure, the distance between wall-based ground improvement columns required to prevent liquefaction and the allowable stress on such columns are set in consideration of the related elastic-behavior limitations. However, the concept of allowing plastic deformation and local failure of these columns in strong earthquakes may be considered in view of cost-effectiveness as long as the relevant functions (usability, repairability and safety) are preserved.

The constitutive law of an elastic and perfectly plastic body allows the setting of failure strength but does not support calculation of strain-softening observed with ground improvement columns after failure. Accordingly, in relation to failure phenomena, there is a need for a constitutive law that allows calculation of strain-softening characteristics. The law proposed by Namikawa and Mihira (2007) supports the setting of criteria for shear and tensile failure as well as calculation of strain-softening at the post-failure stage. With this model, the results of experimentation and numerical simulation using test-pieces of cement-treated sand were compared. However, the model was not examined in terms of validity for body improvement via jet grouting, which creates strength variations inside ground improvement columns.

In this study, the authors compared the results of unconfined compression testing for ϕ 300 mm core samples created with jet grouting and the outcomes of numerical simulation to examine the validity of the constitutive law. It was assumed that ground improvement bodies are characterized by strength variability based on the method proposed by Morikawa et al.

(2013). A 3D FEM model of lattice-based ground improvement was then created, and countermeasures for the effects of liquefaction occurring upon local failure in improved ground after a strong earthquake were considered. A parametric approach involving variations in wall distance, wall thickness and the constitutive law was adopted.

The elasto-plastic model was utilized with a user-supplied subroutine function of the DIANA 10.1 FEM analysis program (DIANA FEA B.V. 2016).

2 CONSTITUTIVE LAW FOR CEMENT-TREATED SAND

The elasto-plastic model proposed by Namikawa and Mihira (2007) as a constitutive law for cement-treated sand involves criteria for shear failure and tensile failure. Namikawa and Koseki (2006) compared experimental and analysis results obtained using different test methods and examined the validity of the constitutive law based on the outcomes.

The model expresses strain-softening with reduced post-peak stress for shear and tensile failure, and can reproduce shear behavior involving strain-hardening with no clear peak stress. Cement-treated sand is described with 14 model parameters, including rigidity, shear strength, tensile strength, the post-peak stress-strain relationship and shear-zone width (i.e. the width of cracks in cement-treated sand).

3 UNCONFINED COMPRESSION TEST ANALYSIS

3.1 *Purpose*

The analysis involved strength testing of ground improvement columns, calibration of simulation parameters from the test results, and examination of the constitutive law's validity.

There are spatial variations of strength inside ground improvement columns, which sometimes contain non-solidified areas (Architectural Institute of Japan 2006 and Building Center of Japan 2002) (Figure 1 a, b). As such columns have diameters as large as several meters, experimentation using actual columns has been limited. In ex-post evaluation, cores are often collected (Figure 1 c) and unconfined compression tests are performed, although only for solidified parts. In this study, it was necessary to consider the presence of solidified and non-solidified parts in an attempt to express the overall strength of improved ground.

3.2 *Analysis*

Variations in the strength of solidified material were considered using a statistical method (Deutsch et al. 1992), and the ratio of non-solidified material was calculated using data from a small-diameter core. The resulting data were adopted in numerical analysis, whose results were then compared with the outcomes of strength testing on a large-diameter core.

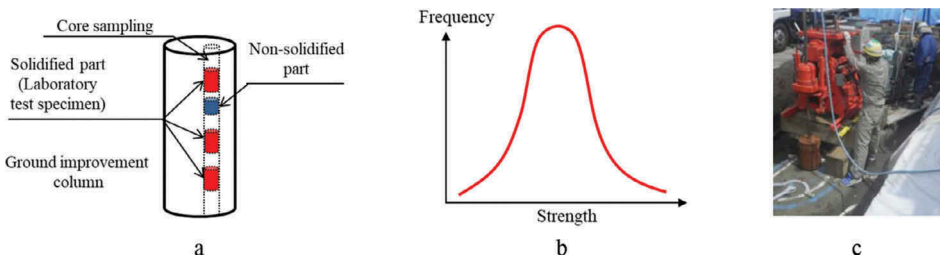

Figure 1. a) Ground improvement column and core sampling. b) Schematic illustration of small-diameter core strength distribution. c) Collection of large-diameter core

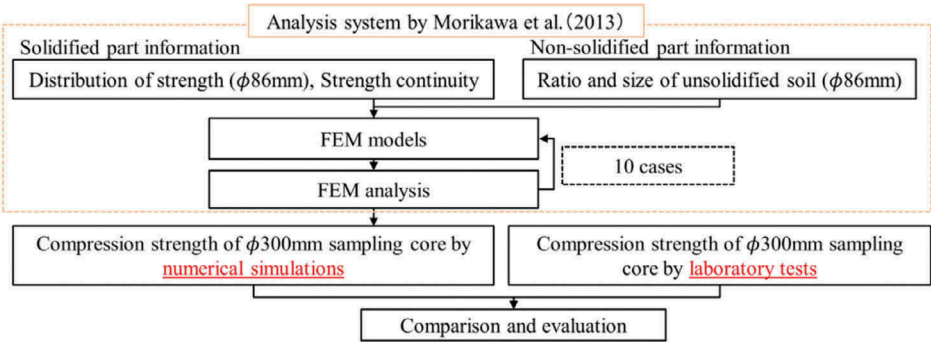

Figure 2. Flow of analysis procedure

Table 1. Non-solidification ratio and size of non-solidified parts

Item	Non-solidification ratio*	Average size of non-solidified parts
	%	mm
Measurement value	3.0	30

* For parts with 50% non-solidification in the core cross section

The analysis procedure is shown in Figure 2. The method of strength variation evaluation for ground improvement columns developed by Morikawa et al. (2013) was used to set the spatial variation of strength in FEM analysis. This method takes into account the previously mentioned non-solidification ratio, the average size of non-solidified parts, the results of unconfined compression testing on small-diameter cores, and strength continuity as determined via needle penetration testing. The strength of large-diameter cores can be estimated using Monte Carlo simulation with this model. The elasto-plastic model was used for the ground improvement column constitutive law. In the present experiment, unconfined compression testing of large-diameter cores was conducted separately and the validity of the model was checked by comparing numerical and experimental results.

3.2.1 *Jet grouting and core sampling*

Ground improvement columns were made as per the actual construction method (jet grouting), and cores with diameters of 86 and 300 mm were collected after solidification. Non-solidification in the ϕ86 mm cores was judged if the non-solidified area accounted for more than 50% of the cross section. The non-solidification ratio and average size of non-solidified parts are shown in Table 1. The non-solidification ratio is the percentage of non-solidified volume to the total core volume.

3.2.2 *Unconfined compression test results*

The results of the unconfined compression testing conducted on the ϕ86 and ϕ300 mm cores (Figure 3, Table 2) indicate higher average strength among the ϕ86 mm samples (Iguchi et al. 2018). This is attributed to non-solidified content and spatial variations in the strength of the solidified parts. Max. and Min. in Table 2 indicate the maximum and minimum compressive strength.

3.2.3 *Needle penetration test*

Needle penetration testing (Figure 4 a) was conducted to determine the hard-soft part ratio and the strength continuity of ground improved columns with ϕ300 mm cores immediately after extraction with depth intervals of 50 mm. Four side lines with angle intervals of 90 degrees were also set on the specimen to support related measurement (Figure 4 b). The penetration force determined was divided by the penetration length to calculate the needle penetration gradient representing penetration resistance.

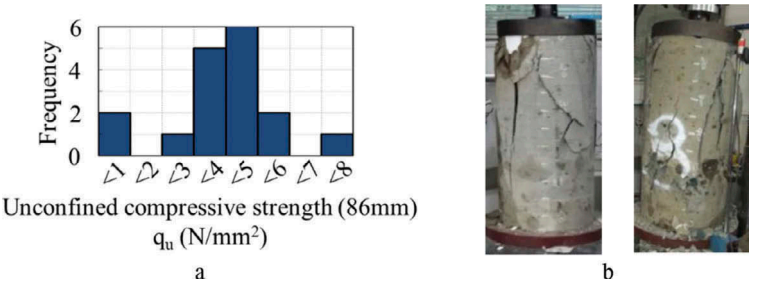

Figure 3. a) Strength distribution in small-diameter cores (ϕ86 mm). b) Unconfined compression test for large-diameter cores (ϕ300 mm)

Table 2. Results of unconfined compression testing

Core diameter	Number of samples	Max.	Min.	Average	Coefficient of variation
mm		N/mm^2	N/mm^2	N/mm^2	%
86	21	7.3	0.2	4.0	40.2
300	2	3.8	3.7	3.7	-

Figure 4. a) Needle penetration tester. b) Needle penetration points

3.2.4 *Numerical simulation conditions*

A model with the same size as the large-diameter cores was created and the same boundary conditions as those of the unconfined compression test were set. A different strength value was assigned to each element in FEM analysis based on the experimental values (Kawamura et al. 2018) (Figure 5).

3.3 *Numerical simulation results*

Using the elasto-plastic model as the constitutive law with spatial variations in the strength of the ground improvement columns, the results of unconfined compression testing for the columns were reproduced. The numerical results reflected both the peak stress of the samples and strain-softening after peak stress. The region of large strain and the inclined-crack shape were also similar to the experimentally observed results (Figure 6) (Table 3).

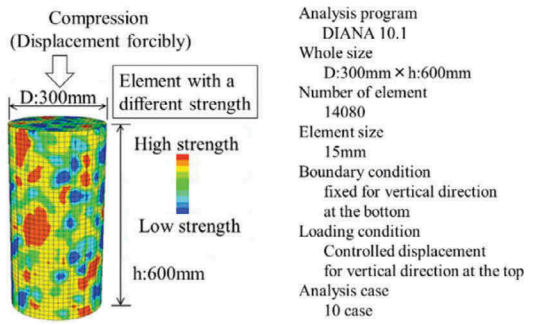

Parameters of the constitutive law

$E = 750q_u\ (N/mm^2)$, $\nu = 0.26\ (-)$

$C = 0.3q_u\ (N/mm^2)$, $\phi = 30\ (degree)$

$T_f = 0.2q_u\ (N/mm^2)$, $e_y = 0.0002\ (-)$

$e_r = 0.4\ (-)$, $\alpha = 1.05\ (-)$

$sftcrv = -T_f{}^2 \times t_{s0}/(0.009 \times q_u/1.7)\ (N/mm^2)$

$D_c = 0.4\ (-)$, $l_c = 15\ (mm)$

$t_{s0} = 0.6\ (mm)$

$tsimin = 0.01\ (-)$, $cohmin = 0.01\ (-)$

Figure 5. Model example and numerical simulation conditions

4 ANALYSIS OF LATTICE-BASED GROUND IMPROVEMENT

4.1 *Purpose*

The elasto-plastic model allows evaluation to determine behavior associated with lattice-based ground improvement and clarification regarding the emergence of local failure conditions. Such analysis is performed to identify areas of local failure and weaknesses in lattice-based ground improvement, and also helps to elucidate variations in the effects of liquefaction resistance after local failure.

4.2 *Analysis*

Lattice-based ground improvement usually targets an improvement ratio of 50% for plane areas or above based on previous studies indicating the effectiveness of liquefaction countermeasure application. Analysis in the present study covered both the ordinary improvement ratio and a lower ratio to determine the effects of liquefaction countermeasures after the occurrence of local failure. Calculation was also implemented for ground improvement columns defined with a linear model for comparison with the elasto-plastic model. A total of six cases were considered (Table 4).

Definition of ground conditions was based on the liquefaction layer above 10 m in depth and the non-liquefaction layer below 10 m. The SPT N value was set as 10 for the upper 5 m part of the liquefaction layer and as 15 for the lower 5 m part, and as 30 for the non-liquefaction layer (Figure 7). The density of the ground and of the ground improvement columns were both assumed to be 1.8 g/cm^3. For the boundary between the original soil and the ground improvement columns, interface elements capable of opening when loaded in tension were used. The soil-wall friction angle was assumed to be 2/3 of the internal soil friction angle. For the ground improvement columns, parameters were set with an assumed unconfined compression strength of q_u = 2 N/mm^2.

The gravity load was applied to the entire model, and a horizontal inertial force was then gradually applied at intervals of K_h = 0.0005 until K_h = 0.35.

The mesh domain used for the analysis was determined to model half of the lattice-based ground improvement domain. For the boundary conditions, the bottom was fixed and the long side face was fixed in the direction perpendicular to the load. The boundary condition for the short side faces was defined so that displacement on both sides was equal. In an actual-size model, strength variability couldn't be considered.

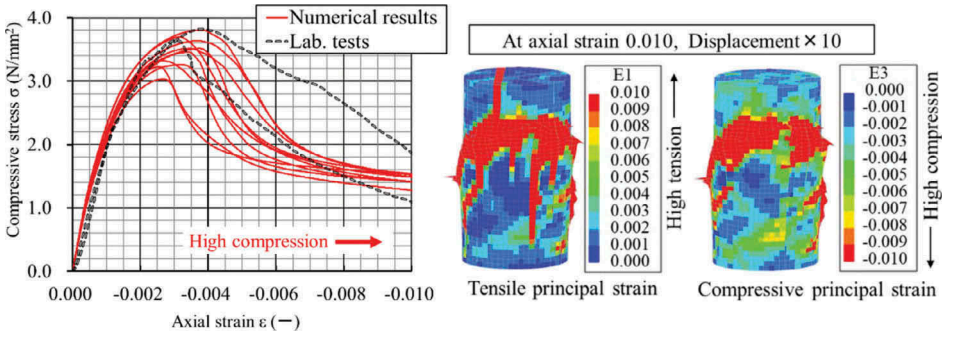

Figure 6. Comparison of laboratory testing and numerical results for unconfined compression testing

Table 3. Results of experimentation and numerical analysis

Item	Unconfined compressive strength
	N/mm^2
Experimental results (ϕ300 mm)	3.65 – 3.82 (average 3.74)
Numerical results (ϕ300 mm)	3.03 – 3.80 (average 3.45)
(Reference) Experimental results (ϕ86 mm)	0.20 – 7.34 (average 4.04)

Table 4. Calculation cases

Improvement ratio*	Wall thickness	Distance between wall centers	Constitutive law of improvement
%	m	m	
19	1	10	Elasto-plastic model, linear model
36	2	10	Elasto-plastic model, linear model
56	2	6	Elasto-plastic model, linear model

* Improvement ratio: ((wall-center distance)^2-(inside-wall distance)^2)/(wall-center distance)^2

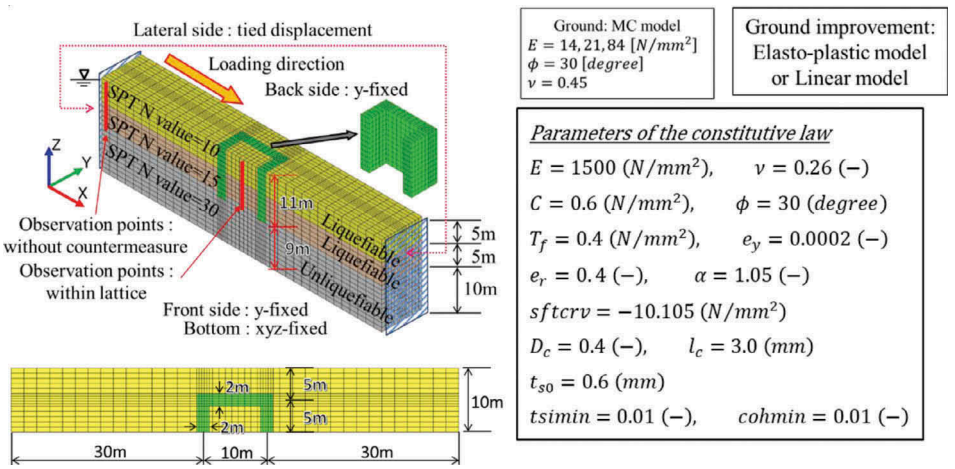

Figure 7. Example of analysis model (improvement ratio: $(10^2–8^2)/10^2\times100 = 36\%$)

4.3 *Numerical simulation results*

Outlined below are the results of liquefaction analysis at different depths based on subterranean shear stress data. The term "without countermeasure" denotes consideration outside lattice-based ground improvement columns and near the model boundary, while "within lattice" denotes consideration of non-improved central ground within the lattice of the ground improvement columns (Figure 8). Without the countermeasure, the liquefaction safety factor is below 1 in most areas except near the ground surface, where values are relatively high due to low confining pressure and identical SPT N value. This safety factor is based on the method outlined in Architectural Institute of Japan (2001). Higher liquefaction safety factors were observed inside the lattice as a whole, thereby verifying the effects of improvement based on a lattice structure. The increased improvement ratio was also found to enhance this effect. Conventional design usually involves the setting of an improvement ratio of 50% or higher, but in the present experiment the safety factor exceeded 1 in many areas other than deep parts, and the liquefaction countermeasure was found effective even with an improvement ratio of just 36%.

The tensile principal stress within the lattice is shown in Figure 9. The value was set as 0.4 N/mm^2, and some elements were found to be in a stress state that could result in failure. In particular, this tendency is evident with low improvement ratios. The stress is high on the bottom part and along the wall perpendicular to the load direction, and increases in some places along the wall parallel to the load direction. This perpendicular stress is high due to wall deformation caused by earthquake-related pressure from soil and water.

Figure 10 shows the results of analysis in which a linear elastic body was used to model improved ground, and illustrates elements with higher levels of stress than the preset tensile strength of 0.4 N/mm^2. As there is no limit on loaded stress in the linear elastic body, levels exceeding the tensile strength may occur. This tendency was particularly evident with low

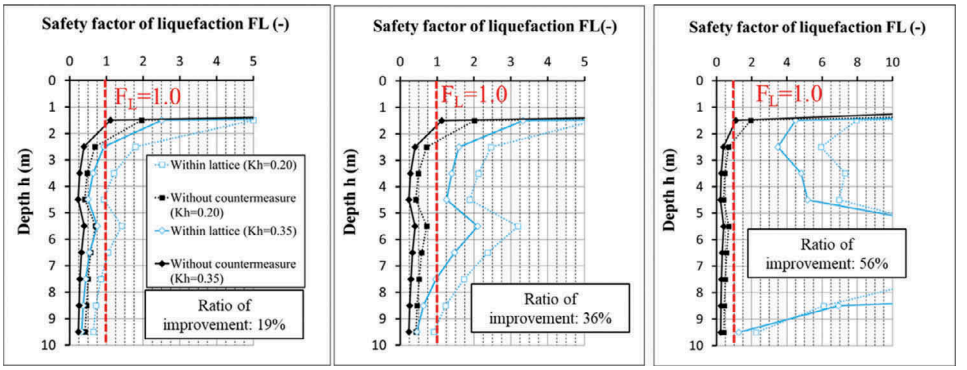

Figure 8. Liquefaction safety factor distribution (elasto-plastic model)

improvement ratios. However, even in such cases, stress exceeding tensile strength occurred in only a few elements for $K_h = 0.20$ but in many elements for $K_h = 0.35$.

Numerical simulation indicated that the top and bottom of the wall perpendicular its corner may be subject to weakening.

Ratios of improvement and the liquefaction safety factor at a depth of 4.5 m are shown in Figure 11. As the liquefaction layer is 10 m deep, 4.5 m is around the central depth.

As detailed above, the liquefaction safety factor was 1 or below without the countermeasure but higher with it. It was also found that an enhanced improvement ratio improved the effects of the countermeasure, and that related effects could be expected even with a ratio of 36%, which is lower than the 50% figure of conventional design.

Comparison of the elasto-plastic model to the linear model indicated that the safety factor of the latter was slightly higher for a low improvement ratio, which may cause widespread failure in strong earthquakes. However, no major difference was observed in the comparison results. This indicates that the liquefaction resistance effect is maintained after failure.

Accordingly, analysis using the linear model is not considered appropriate, whereas application of the elasto-plastic model may be considered effective and appropriate for assessing the characteristics of ground improvement at the post-failure stage.

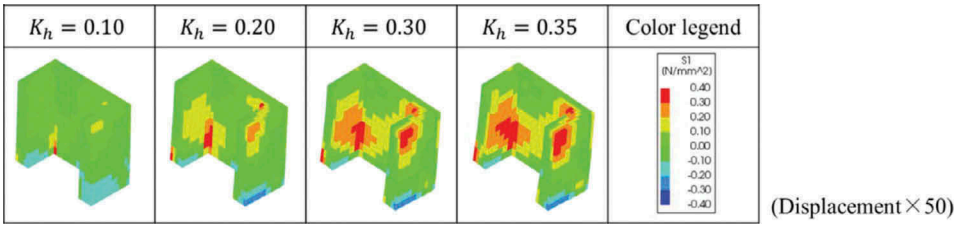

Figure 9. Maximum principal stress with ground improvement (improvement ratio: 19%; elasto-plastic model)

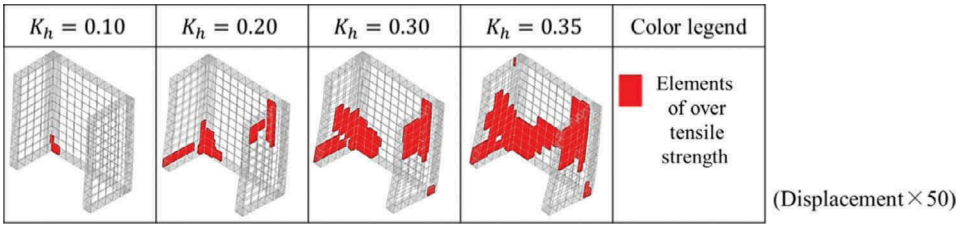

Figure 10. Elements of excess tensile strength (improvement ratio: 19%; linear model)

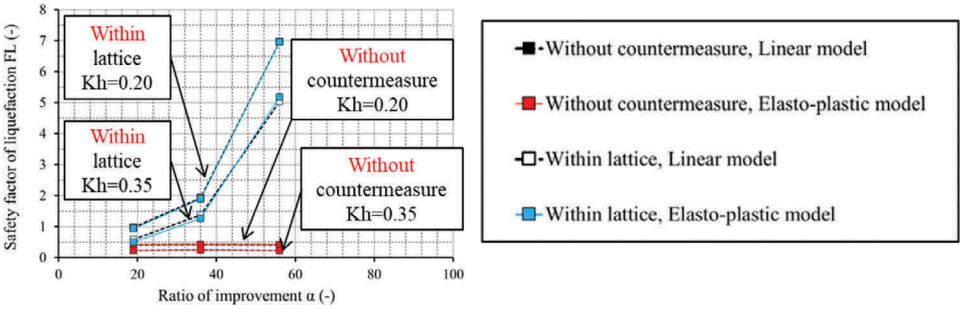

Figure 11. Relationship between improvement ratio and liquefaction safety factor (GL-4.5 m)

5 CONCLUSION

Finite element analysis with unconfined compression testing indicated that the elasto-plastic model proposed by Namikawa and Mihira (2007) can be applied for appropriate calculation to determine the peak strength of actual ground improvement columns and the stress-strain relationship before and after failure. The results of the study also helped to clarify the overall strength of ground improvement measures and indicated the validity of the constitutive law for ground improvement involving jet grouting.

The study additionally helped to clarify the area of local failure and weakened parts in lattice-based ground improvement, and suggested that liquefaction resistance effects are maintained at the post-failure stage. Analysis of improvement indicated that the elasto-plastic model supported evaluation regarding the behavior of lattice-based ground improvement during earthquake conditions, local failure of the improved domain and the effectiveness of the liquefaction countermeasure after the failure of the improved element.

Based on the outcomes of the study, the authors consider practical work combining these two methods feasible.

REFERENCES

Architectural Institute of Japan 2001. *Recommendations for Design of Building Foundations*

Architectural Institute of Japan 2006. *Recommendations for Design of Ground Improvement for Building Foundations*: 43-47&138-140

Building Center of Japan 2002. *Recommendations for Design and Quality Control of Ground Improvement for Building – deep and shallow chemical mixing method*

Deutsch C.V. and Journel A.G. 1992. *Geostatistical Software Library and User's Guide*. Oxford University Press

DIANA FEA B.V. 2016. *DIANA User's Manual Release 10.1 DIANA FEA B.V.*

Iguchi Y. & Kawamura J. 2018. Large scale core sampling and unconfined compression test for ground improvement by jet grouting (in Japanese). *53rd Japan National Conference on Geotechnical Engineering*

Kawamura J. & Iguchi Y. & Namikawa T. & Takehara K. & Yamada T. & Ohno S. 2018. Analysis based on strength distribution and strain softening for ground improvement by jet grouting (in Japanese). *53rd Japan National Conference on Geotechnical Engineering*

Morikawa S. & Namikawa T. & Sakanashi T. & Yazawa F. & Sakota K. & Matsuzaki H. 2013. Development of a rational evaluation technique for ground improvement strength (No. 2) – An evaluation analysis system for ground improvement strength (in Japanese). *48th Japan National Conference on Geotechnical Engineering*

Namikawa T. & Koseki J. 2006. Experimental determination of softening relations for cement-treated sand. *Soils and Foundations Vol. 46 No. 4*: *491-504*, Japanese Geotechnical Society

Namikawa T. & Mihira S. 2007. Elasto-plastic model for cement-treated sand, *International Journal for Numerical and Analytical Methods in Geomechanics*: *71–107*